INSTITUTE OF PHYSICS PUBLISHING JOURNAL OF OPTICS A: PURE AND APPLIED OPTICS

J. Opt. A: Pure Appl. Opt. **8** (2006) S227–S233 doi:10.1088/1464-4258/8/4/S24

# Near-field photonics: tip-enhanced microscopy and spectroscopy on the nanoscale

**Neil Anderson**[1], **Alexandre Bouhelier**[2] **and Lukas Novotny**[1,3]

[1] The Institute of Optics, University of Rochester, Rochester, NY 14627, USA
[2] The Center for Nanoscale Materials, Argonne National Laboratory, Argonne, IL 60439, USA

E-mail: novotny@optics.rochester.edu

Received 28 July 2005, accepted for publication 23 September 2005
Published 24 March 2006
Online at stacks.iop.org/JOptA/8/S227

**Abstract**
Any detailed study of the interaction of electromagnetic radiation with nanoscale systems is limited by diffraction effects in classical optical systems. Near-field microscopy extends conventional imaging beyond this self-imposed barrier and is used to perform microscopy and spectroscopy with ultra-high spatial resolution. In this article we will discuss the use of the enhanced electric field created at the apex of a sharp laser-irradiated metal tip as a means of producing a truly nanoscale light source. This confined light source can be used to excite locally vibrational modes along carbon nanotubes or to investigate surface charge oscillations in optically resonant nanoparticles. We report the use of such a technique to demonstrate localized photofluorescence and Raman imaging with sub 20 nm spatial resolution.

**Keywords:** near-field, single-walled carbon nanotubes, vibrational spectroscopy, gold nanoparticles, plasmons

(Some figures in this article are in colour only in the electronic version)

## 1. Introduction

Studying optical interactions on the nanoscale permits the investigation of a large number of interesting phenomena ranging from light–matter interactions within highly confined systems such as quantum dots and quantum well structures, as well as in biological species such as single molecules and individual proteins [1]. In providing a comprehensive and detailed analysis of such systems it is necessary to probe within nanoscale interaction volumes that are typically on the order of 10–20 nm[3] and as such are inaccessible using conventional light microscopy techniques. One technique that allows such highly localized light–matter interactions is known as tip-enhanced near-field optical microscopy (TENOM).

The first reported work in near-field microscopy using visible light was published independently by two groups led by Pohl [2] and Lewis [3]. In both sets of experiments the light emitted by a tiny aperture, as described earlier by Synge [4], was used to demonstrate optical imaging with a spatial resolution of $\lambda\backslash 20$ compared with $\lambda\backslash 2.5$ using conventional microscopy techniques. In using such aperture probes the first near-field fluorescence imaging of *single* molecules was performed by Betzig and co-workers [5]. However, given the low light transmission of metal coated aperture probes ($\sim 10^{-4}$ for a 100 nm aperture) [6] laser-illuminated metal tips are used as a means to achieve not only improved spatial resolutions (10 nm) but also increased field enhancements and S/N.

There are two distinct types of tip-based imaging:

(i) *tip-scattering microscopy*, where the tip locally perturbs the field close to the sample with both the near-field and far-field contributions detected in the far zone [7, 8];
(ii) *tip-enhanced spectroscopy*, where the laser-illuminated tip locally excites and enhances a spectroscopic response in the sample within a small interaction volume, defined by the tip diameter [9–12].

[3] Author to whom any correspondence should be addressed.

  

In this paper we discuss the application of tip-enhanced microscopy and spectroscopy. We start with a discussion on the field enhancement at sharp metal tips and introduce the general experimental arrangement used. In the remainder of the article we discuss the use of such probes in studying the structural properties of individual single-walled carbon nanotubes (SWNTs) by measuring the local Raman spectrum and the investigation of the intensity distribution surrounding photoexcited resonant gold nanostructures.

## 2. Field enhancement at a sharp metal tip

A key component of tip-enhanced microscopy is the ability to produce highly confined electromagnetic fields (i.e. nanoscale light sources) at the apex of sharp metal tips [13]. The enhanced electromagnetic field originates from a combination of

(1) an electrostatic lightning rod effect, which is a direct result of the geometric singularity of sharply pointed metal structures, and
(2) surface plasmon resonances, which depend on both the excitation wavelength and tip geometry.

The confined electric field is readily produced if the electric field vector of the incident light field is polarized along the direction of the tip shaft. This light field periodically drives the free electrons on the surface of the metal along the direction of polarization i.e. along the longitudinal axis of the tip. The resultant enhanced electric field is confined to a volume on the order of $(20\ \mathrm{nm})^3$, with the confinement volume dependent on the end diameter of the metal tip. If the incident electric field vector is not polarized along the direction of the tip shaft the field enhancement effect is significantly weaker [13].

In the case of Raman scattering induced by nanoscale metal structures [14, 15] the strongest contribution to surface-enhanced Raman scattering (SERS) is electromagnetic in origin. The observed enhancement is caused by the enhancement of the incident field $E_\mathrm{i}$ at $\omega_\mathrm{i}$, and the scattered field $E_\mathrm{s}$ at $\omega_\mathrm{i}$–$\omega_\mathrm{v}$, where $\omega_\mathrm{v}$ is a vibrational frequency. The enhancement factor $M$ is then expressed as the product with the total electric field $E_\mathrm{t}$:

$$M = \left[\frac{E_\mathrm{t}(\omega_\mathrm{i})}{E_\mathrm{i}(\omega_\mathrm{i})}\right]^2 \left[\frac{E_\mathrm{t}(\omega_\mathrm{i}-\omega_\mathrm{v})}{E_\mathrm{i}(\omega_\mathrm{i}-\omega_\mathrm{v})}\right]^2 \simeq \left[\frac{E_\mathrm{t}(\omega_\mathrm{i})}{E_\mathrm{i}(\omega_\mathrm{i})}\right]^4 \qquad (1)$$

where we have taken $\omega_\mathrm{v} \ll \omega_\mathrm{i}$.

It has been determined that the local field near a laser-irradiated tip can be approximated by the electric field of an effective dipole $\mathbf{p}(\omega)$ located at the centre of the tip apex. The magnitude of the effective dipole can be written as [16]

$$\mathbf{p}(\omega) = \begin{bmatrix} \alpha_\perp & 0 & 0 \\ 0 & \alpha_\perp & 0 \\ 0 & 0 & \alpha_\parallel \end{bmatrix} \mathbf{E}_0(\omega) \qquad (2)$$

where we chose the $z$-axis to coincide with the tip axis and $\mathbf{E}_0$ is the exciting electric field in the absence of the tip. The transverse polarizability $\alpha_\perp$ is identical to the quasi-static polarizability of a small sphere whereas the longitudinal polarizability $\alpha_\parallel$ is given by

$$\alpha_\parallel(\omega) = 8\pi\varepsilon_0 r_0^3\, f_\mathrm{e}(\omega) \qquad (3)$$

where $r_0$ is the tip radius and $f_\mathrm{e}$ the complex field enhancement factor. Thus, the enhancement at the tip generates locally a light source which can be accurately represented by a single on-axis oscillating dipole [16, 17]. The dipole strength is a direct measure for the field enhancement factor.

## 3. Experimental set-up

Our tip-enhanced microscopy set-up is based on an inverted optical microscope fitted with an $x$, $y$-stage for raster scanning samples. We employ two different sets of excitation sources. For our near-field Raman studies we use a tunable dye laser pumped by a high-power solid-state laser. In another similar configuration we use a mode-locked Ti:sapphire laser producing 150 fs laser pulses at 780 nm to study non-linear optical processes such as two-photon absorption. In both configurations linearly polarized Gaussian beams can be tailored using a mode converter to produce radially symmetric (doughnut) modes [18] as well as Hermite–Gaussian modes. The advantage in using certain higher order laser beams lies in the increased strength of the longitudinal field components that provide the necessary polarization condition for driving the field enhancement effect. The mode-converted laser beam is then reflected using a beam splitter and focused onto the sample by means of a high numerical aperture oil immersion lens (NA = 1.4) as shown in figure 1. Having obtained a tight focus at the sample surface, a sharp metal tip is placed in the focal region. The tip is held in a constant height mode of 2 nm from the sample surface by means of a shear-force feedback scheme [19]. In order to produce the desired field enhancement at the tip apex, the tip must couple with one of the longitudinal field lobes. For a Gaussian beam, there are two such longitudinal field components that are located off-centre, one on either side of the centre in the direction of the incident polarization. For a radially polarized beam a single longitudinal field lobe is located in the centre of the focused laser spot and therefore no displacement of the gold tip is necessary. Using the $x$, $y$-scan stage we then raster scan the sample, maintaining the tip at a fixed position with respect to the optical axis. The emitted photoluminescence or Raman scattered light is collected by the same microscope objective, transmitted through the beam splitter and detected using either a single-photon avalanche photodiode (APD) or a charged-coupled device (CCD) cooled to $-124\,^\circ\mathrm{C}$. Typical acquisition times are on the order of tens to hundreds of milliseconds per image pixel. In our studies we use high-purity (99.998%) gold wire electrochemically etched in a bath of HCl to an end diameter of 10–20 nm.

## 4. Applications of near-field microscopy

### *4.1. Near-field Raman microscopy of single-wall carbon nanotubes*

Tip-enhanced optical microscopy offers the opportunity to study the intrinsic molecular structure of many (manmade or naturally occurring) nanoscale systems [20, 21], reporting detailed spectroscopic information with a spatial resolution on the length scale of only a few tens of atom–atom bond lengths. To this end tip-enhanced Raman spectroscopy is

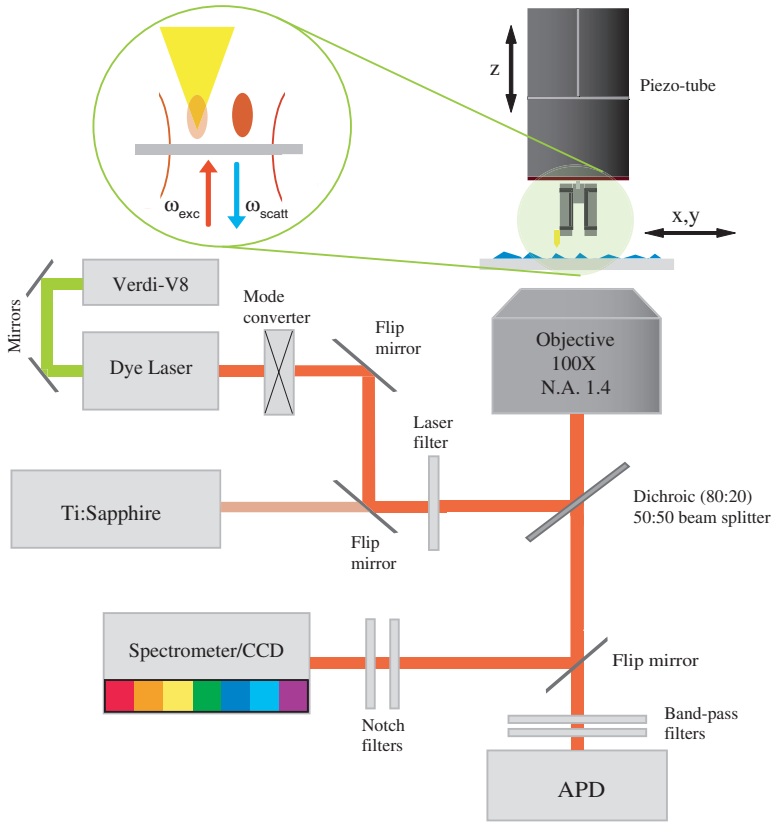


**Figure 1.** Schematic diagram of both experimental configurations used in our tip-enhanced studies. A sharp metal tip is coupled to the longitudinal field component of the laser spot and the sample is scanned laterally. Shown are the two longitudinal field lobes of a linearly polarized Gaussian beam. The scattered light is detected using either an APD or a combination of a spectrograph and cooled CCD.

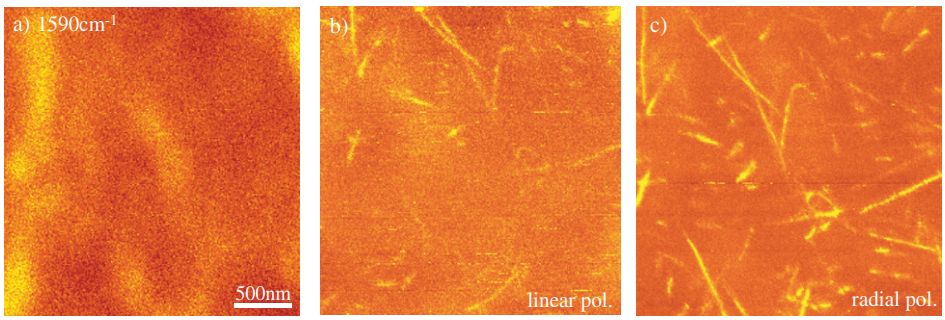


**Figure 2.** Raman scattering images of single-walled carbon nanotubes resting on a glass cover slip. The contrast in the images reflects the local intensity of the Raman G band (1590 $cm^{-1}$). (a) Confocal Raman image; (b) corresponding tip-enhanced Raman image using a linearly polarized Gaussian beam and (c) tip-enhanced Raman image acquired using a radially polarized laser beam. The integration time per image pixel was 10 ms. The offset in images (b) and (c) is a result of retracting the tip and aligning the optical path of the radial mode then approaching the tip to the sample surface.

ideally suited to the study and optical characterization of single-wall carbon nanotubes (SWNTs) [9, 22]. In this section we discuss our recent near-field Raman studies of SWNTs where we display the key characteristics of tip-enhanced imaging, namely high spatial resolution and localized field enhancement. In addition, we will show how tip-enhanced spectroscopy can be used to map vibrational modes along individual SWNTs and identify *localized* Raman scattering not seen using conventional confocal Raman spectroscopic techniques.

Figure 2(a) shows a confocal Raman image of a dispersion of arc-discharge SWNTs on a glass coverslip (FWHM $\sim$ 280 nm) accompanied by two tip-enhanced Raman images acquired over the same sample area using a linearly polarized Gaussian beam ($TEM_{00}$)(b); and a radially polarized beam (c) respectively. The same gold tip (diameter $\sim$ 30 nm) was used in acquiring both images (b) and (c). We clearly observe an improved image contrast when the tip couples to the longitudinal component of a radially polarized laser beam. This result is to be expected since it is known that the $z$-field

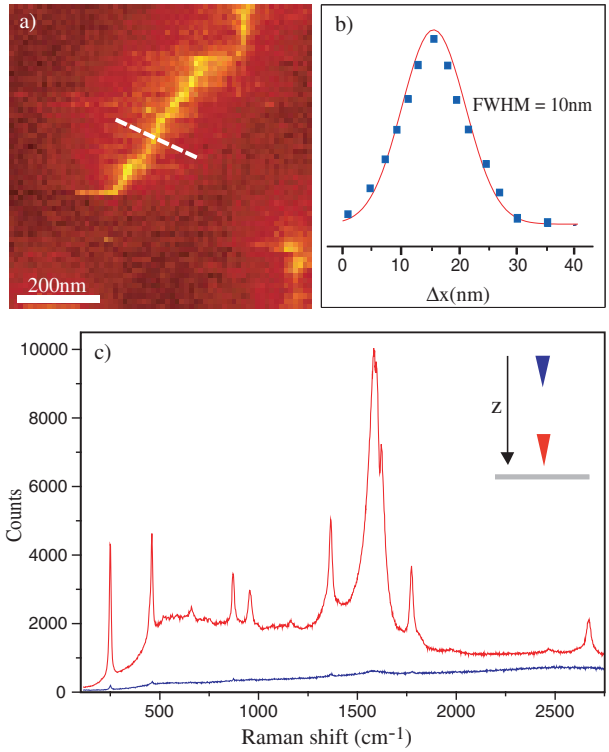


**Figure 3.** Raman scattering image of an arc-discharge SWNT: (a) near-field Raman image over spectral range centred at $\nu = 2600\ \mathrm{cm}^{-1}$ (G′ band); (b) cross section taken along the dashed line in the Raman image revealing a optical resolution of 10 nm and (c) tip-enhanced Raman spectrum acquired from an individual SWNT; the Raman modes of the SWNT are significantly enhanced in the presence of a sharp metal tip (grey/red) compared to the case when the tip is withdrawn (black/blue). From this measurement we estimate an enhancement factor of $10^6$. The increased background is due to luminescence generated by the gold tip.

of a radially polarized mode is significantly stronger than for a lower order Gaussian mode.

The average spatial resolution obtained in both figures 2(b) and (c) was on the order of 20 nm. However, with careful control over the tip fabrication process it is possible to produce sharp metal tips with end diameters on the order of 15–20 nm. In using such sharp tips it is possible to extend the spatial resolution down to 10 nm as can be seen in figures 3(a) and (b). Figure 3(c) shows the enhanced Raman spectrum acquired from the SWNT shown in figure 3(a). Two sets of spectra are acquired. The first measurement is taken with the gold tip fully retracted ($\sim$1.5 $\mu$m) from the sample surface (blue) and a second measurement with the tip held at a constant height of 2 nm at one point along the SWNT (red). By taking into account the ratio of both the confocal and near-field interaction areas we determine the Raman enhancement factor to be $\sim 10^6$.

The spectroscopic properties of carbon nanotube structures have been studied extensively in the literature [23–27]. Many confocal (far-field) Raman studies of SWNTs have provided a wealth of useful information from which to determine structural characteristics such as nanotube diameter and chirality $(n, m)$ (i.e. metallic or semiconducting CNTs) [28, 29]. However the detected Raman scattered light is taken as the average signal detected within the size range of a typical diffraction limited laser spot (500–1000 nm). To date a detailed and comprehensive chemical analysis of SWNTs with sub-wavelength resolution has been lacking. With near-field (tip-enhanced) Raman spectroscopy one can now readily characterize individual SWNT structures via variations in their local Raman spectrum [22]. Any such variations may be attributed to local environmental effects, the presence of defects in the nanotube lattice and variations in SWNTs synthesized by different growth processes (e.g. arc-discharge and CVD).

The vibrational spectrum of a carbon nanotube is a unique chemical fingerprint with which to identify the nanotube structure. By measuring the spectral position of the outward radial breathing mode of the carbon atoms in the nanotube lattice (RBM, 100–300 $\mathrm{cm}^{-1}$) (or the spectral position of the tangential stretching mode (G band), $\sim$1590 $\mathrm{cm}^{-1}$), one can determine the nanotube chirality $(n, m)$ and diameter $d_t$. To determine the extent of local defects we study disorder-induced Raman scattering $\sim$1300 $\mathrm{cm}^{-1}$ (D band). Other interesting phonon modes are found in the spectral region $\sim$600–1100 $\mathrm{cm}^{-1}$ and are known as intermediate-frequency modes (IFMs) [30, 31]. From our own near-field studies we have observed highly localized disorder-induced IFM scattering, indicating a possible link between the origin of these phonon modes in carbon nanotubes.

Figure 4 shows a series of near-field images acquired over the spectral regions (a) 1585 $\mathrm{cm}^{-1}$ (G band), (b) 1300 $\mathrm{cm}^{-1}$ (D band), (c) 224 $\mathrm{cm}^{-1}$ (RBM) and (d) 837 $\mathrm{cm}^{-1}$ (IFM) respectively for an arc-discharge SWNT. From the spectral position of the RBM frequency we determine the SWNT is metallic with structural indices (13, 1) [32].

From figure 4 we observe a near-uniform spatial profile of the G band with increased Raman scattering located at the beginning of the SWNT. (The G′ band also showed a similar spatial profile along the nanotube. Image not shown.) This is in stark contrast with the other vibrational modes imaged. We clearly observe localized Raman scattering associated with the disorder-induced D band, RBM and IFM and this is consistent with previous results on many different SWNTs synthesized by arc discharge [22]. Figure 4(b) reveals spatially distinct regions along the SWNT where we measure increased disorder-induced (D band) scattering and attribute this to an increased number of spatially localized defect sites in the nanotube sidewall. Furthermore, we observe significant amounts of Raman scattering associated with the IFM mode at 837 $\mathrm{cm}^{-1}$. Typically long integration times (several minutes) are required to detect IFMs in SWNTs using standard confocal Raman spectroscopy techniques [31]. Using our tip-enhanced technique we are able to detect these intermediate frequency modes with timescales on the order of 210 ms. As is shown in figures 4(b), (c) and (d) respectively we observe IFM scattering only in the presence of detectable amounts of defect-induced scattering from SWNTs. This result is consistent with similar measurements on CVD-grown SWNTs and clearly reveals a link between strong IFM and defect-induced Raman scattering in SWNTs [22]. In figures 4(e) and (f) we show the spatial extent of the graphite-like G band at 1582 $\mathrm{cm}^{-1}$ and RBM at 149 $\mathrm{cm}^{-1}$ from a single CVD-grown nanotube resting on a quartz substrate. The most striking feature is the uniformity of the phonon modes along the nanotube and is in direct contrast to

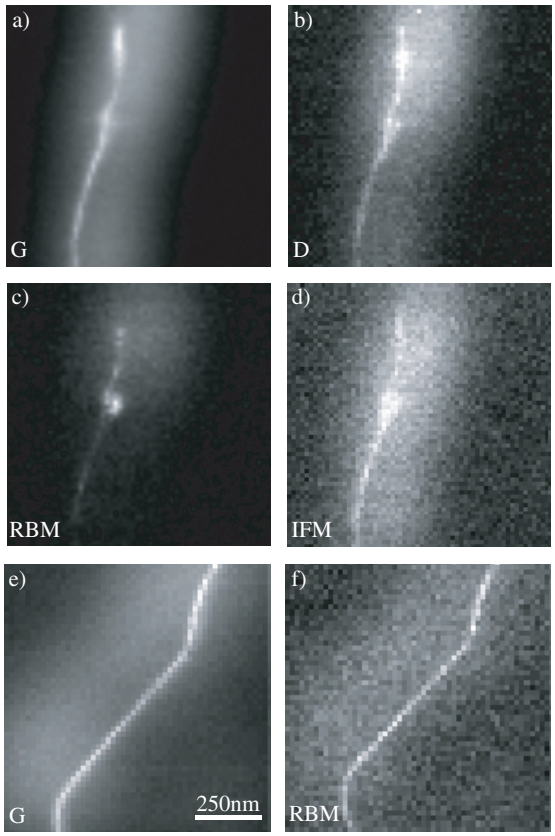


**Figure 4.** Raman scattering images of an arc-discharge SWNT acquired over the following spectral regions: (a) 1585 $cm^{-1}$ (G band); (b) 1306 $cm^{-1}$ (D band); (c) 224 $cm^{-1}$ (RBM) and (d) IFM (837 $cm^{-1}$) respectively. From the measured RBM frequency of 224 $cm^{-1}$ for the arc-discharge nanotube we assign a nanotube structure of (13, 1). Both (e) (1582 $cm^{-1}$) and (f) (149 $cm^{-1}$) are tip-enhanced images of a CVD-grown nanotube. For the measured RBM frequency of 149 $cm^{-1}$ we determine a tube structure of (15, 9). The inset in (f) shows the simultaneously acquired topographic image. The integration time per image pixel was 210 ms.

our results on arc-discharge SWNTs. For the CVD SWNT we observed no detectable defect-induced Raman scattering, even for integration times of several seconds revealing the defect-free nature of SWNTs grown by this process.

Changes in the nanotube structure can occur during growth or purification and can manifest as localized RBM scattering which we observe in many arc-discharge SWNTs. Changes in $(n, m)$ along the nanotube sidewall will result in regions of varying diameter on the order of 0.1–0.2 nm and thus lead to the detuning of the resonance condition with our excitation source $E_{\mathrm{exc}} = 1.96$ eV ($\lambda = 633$ nm). Typical rms noise values of our tip–tuning fork set-up are on the same length scale and therefore such small height variations are difficult to image using a shear-force detection scheme. For the case of CVD-grown SWNTs no such dramatic localization of the RBM has been observed [22, 33].

### *4.2. Field localization in resonant gold nanostructures*

While the contribution of surface plasmons in the local enhancement occurring at metal tips is difficult to quantify, the case of metal nanoparticles has been the subject of intense research in the past. The optical properties of metal nanoparticles are strongly influenced by the surface plasmon resonance [34].

In the electrostatic limit, the polarizability $\alpha_j$ of an ellipsoidal metal particle (permittivity $\epsilon = \epsilon' + \mathrm{i}\epsilon''$) excited by an electric field vector parallel to one of the principal axes $d_j$ ($j = 1, 2, 3$) can be written as

$$\alpha_j = \frac{4\pi v}{3} \frac{\epsilon - \epsilon_{\mathrm{d}}}{\epsilon_{\mathrm{d}} + L_j(\epsilon - \epsilon_{\mathrm{d}})}, \tag{4}$$

where $\epsilon_{\mathrm{d}}$ is the permittivity of surrounding dielectric, $L_j$ is a geometrical factor and $v$ is the volume of the ellipsoid [35]. The poles associated with each axis $d_j$ define the conditions for plasmonic resonances:

$$\epsilon = \epsilon_{\mathrm{d}} \left(1 - \frac{1}{L_j}\right). \tag{5}$$

Surface plasmon resonances in metal particles offer exciting opportunities to control light at the nanometre scale. While the far-field attributes of resonant structures have been extensively studied in the past [34, 35], the appreciation and richness of the optical near field that extends only a few tens of nanometres from the metal surface is in its infancy. With the improvement of high-resolution near-field techniques (see the review by Wiederrecht [36]), fabrication technologies and theoretical understanding [37], our knowledge of single-particle properties is a crucial element for their utilization in more complex structures [38, 39], hybrid systems [40] and devices [41]. Phase-sensitive spectroscopy [42] and imaging [43] as well as mapping of the plasmon modes [44, 45] and their ultrafast dynamics [46] are among the recent advances in our understanding of single resonant metal nanoparticles. In this section we discuss our recent work studying photoluminescent properties of gold nanoparticles under ultrafast illumination.

Local field enhancement due to surface plasmon resonances has been found to be a prerequisite to trigger nonlinear responses from supporting materials. In particular, two-photon induced photoluminescence in rough films [47], metal nanoparticles [48], or optical antennas [49, 50] has been shown to be sensitive to the strength of the local electromagnetic field. Visible photoluminescence in gold originates from interband transitions between occupied d-band electrons and the partially filled sp conduction band. The recombination of the holes with the electrons near the Fermi surface gives rise to the emission of a photoluminescent continuum that is closely related to the surface plasmon resonance. An example of photoexcited luminescence is shown in figure 5(a). The image represents a confocal map of the photoluminescence intensity emitted from an isolated gold nanorod [44]. The intensity distribution was obtained by laterally scanning the particle through the diffraction-limited spot of a focused femtosecond laser beam (150 fs, $\lambda = 780$ nm).

A high-resolution map of the distribution of the local fields surrounding the particle can be recorded by locally scattering the photoluminescence intensity using a sharp metal tip. In contrast to the high-resolution Raman imaging discussed previously, the tip is centred in the focal spot, and in the

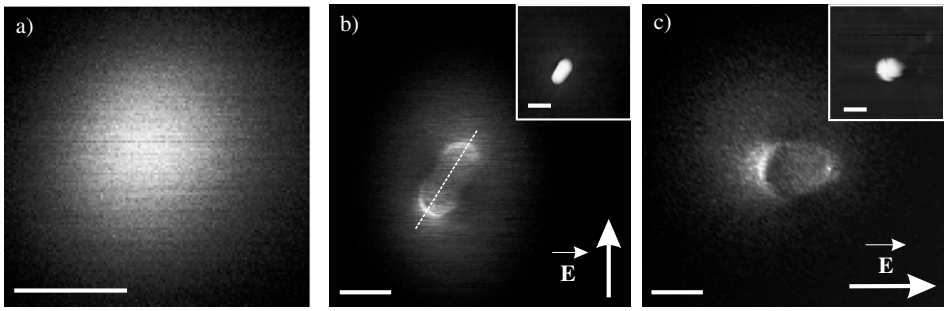


**Figure 5.** (a) Two-photon excited photoluminescence image of a single gold nanorod scanned in the focal plane of a pulsed Gaussian beam. (b) High-resolution near-field photoluminescence image of the same nanoparticle imaged with a stationary gold tip. The inset represents the topography of the rod. (c) High-resolution near-field photoluminescence image of a large spherical gold nanoparticle and its topography (inset). The polarization of the incident electric field vector is indicated by the arrows. The scale bar is 300 nm in (a) and 100 nm in (b) and (c).

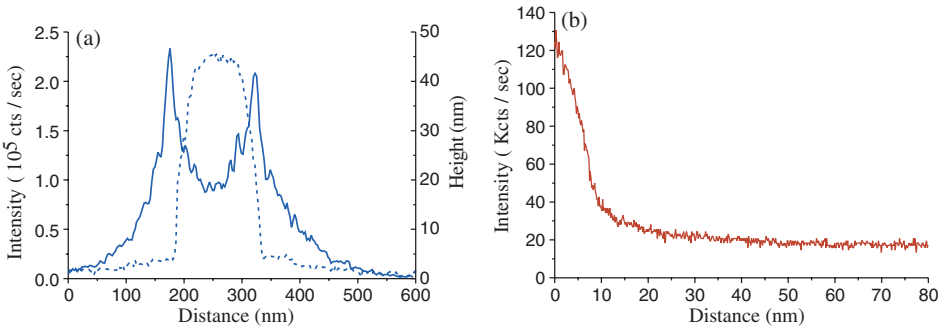


**Figure 6.** (a) Cross-section of the photoluminescence (solid curve) and topography (dashed curve) taken along the long axis of the nanorod of figure 5(b). (b) Photoluminescence decay on top of one the field maxima shown in figure 5(b) as a function of tip–particle vertical separation. The luminescence enhancement is confined to a volume of 1000 $nm^3$.

case of Gaussian excitation no field-enhancement effect is expected as the tip is not coupled to one of the two longitudinal field components. Consequently, the tip can be considered as a passive probe. Figure 5(b) shows the photoluminescence intensity distribution of the same photoexcited gold nanorod as in figure 5(a). In this case a gold tip was held stationary with respect to the optical axis, and the particle was scanned through the focal spot. A similar image is shown in figure 5(c) for a spherical gold particle. The insets in figures 5(b) and (c) show the simultaneously acquired topography of the particles. The arrows represent the polarization of the excitation electric field vector.

The original far field (confocal) photoluminescence patterns similar to figure 5(a) remain visible as a faint background in both figures 5(b) and (c) respectively. Superimposed on this background are high spatial resolution details originating from the tip–particle interaction. At the extremities of the nanoparticles, the photoluminescence response is strongly enhanced relative to the far field photoluminescence. On the other hand, the signal intensity is reduced at the two diametrically opposed points. This is particularly obvious along the short axis of the gold nanorod in figure 5(b). The images demonstrate the dipolar character of the excited particle, namely charge accumulation at both ends along the polarization direction and charge depletion along the perpendicular axis. Cross-sections taken along the long axis of the particle of figure 5(b) are plotted in figure 6(a). The solid curve represents the photoluminescence signal whereas the dashed curve is the topographic profile at the same location. The widths of the photoluminescence peaks at the nanorod extremities are approximatively 17 nm (FWHM), indicating a high degree of confinement. The near-field enhancement becomes evident for tip–particle separations less than 10 nm. This is consistent with the very fast decay of the photoluminescence when the tip is pulled away from the particle as depicted in figure 6(b). Similar tip–sample distance curves are obtained when probing the near-field contrast in our tip-enhanced Raman studies.

## 5. Summary

Near-field microscopy holds great promise for the study and interrogation of a wide variety of nanoscale systems, ranging from probing phonon confinement in low-dimensional nanostructures to the study of individual protein structures embedded in a host membrane. A key component of the technique is the production of nanoscale probes that are able to not only produce strongly enhanced light fields but that can also be used in a wide variety of sample environments and provide good S/N. In using sharp metal tips we have demonstrated the ability to probe light–matter interactions involving nanoscale structures with high spatial resolutions (10 nm). Our studies of Raman scattering in SWNTs have shown the ability of tip-enhanced spectroscopy to produce

vibrational maps that relate directly the local structure of the nanotube lattice. Furthermore, we have demonstrated that tip-enhanced optical imaging can be successfully employed to characterize plasmonic nanostructures. A direct map of the distribution of local fields (hot spots) can be recorded by locally scattering the photoexcited luminescence intensity using a metal tip. Future improvements in both tip design and material properties should permit spatial resolutions below 10 nm.

## Acknowledgments

The authors wish to acknowledge valuable input from Achim Hartschuh and Michael Beversluis. The authors would also like to thank Steve Cronin for providing CVD-grown SWNT samples. This work was funded by the US Department of Energy (DE-FG02-01ER15204) and the Air Force Office of Scientific Research (F-49620-03-1-0379).

## References

[1] Jutamulia S 2002 *Selected Papers on Near-field Optics* (*SPIE Milestone Series* vol 172) (Bellingham, WA: SPIE Optical Engineering Press)
[2] Pohl D W, Denk W and Lanz M 1984 *Appl. Phys. Lett.* **4** 651
[3] Lewis A, Issacson M, Harootunian A and Murray A 1984 *Ultramicroscopy* **13** 227
[4] Synge E H 1928 *Phil. Mag.* **6** 361
[5] Betzig E and Chichester R J 1993 *Science* **262** 1422
[6] Novotny L and Pohl D W 1995 *NATO Adv. Stud. Inst.* E **184** 21
[7] Knoll B and Keilmann F 1999 *Nature* **399** 134
[8] Taubner T, Hillenbrand R and Keilmann F 2004 *Appl. Phys. Lett.* **85** 5064
[9] Hartschuh A, Sanchéz E J, Xie S X and Novotny L 2003 *Phys. Rev. Lett.* **90** 095503
[10] Hayazawa N, Inouye Y, Sekkat Z and Kawata S 2002 *J. Chem. Phys.* **117** 1296
[11] Stöckle S M, Suh Y D, Deckert V and Zenobi R 2000 *Chem. Phys. Lett.* **318** 131
[12] Sanchèz E J, Novotny L and Xie X S 2000 *Phys. Rev. Lett.* **82** 4014
[13] Novotny L, Bain R X and Xie X S 1997 *Phys. Rev. Lett.* **79** 645
[14] Wessel J 1985 *J. Opt. Soc. Am.* B **2** 1538
[15] Nie S and Emroy S R 1997 *Science* **275** 1102
[16] Bouhelier A, Beversluis M R, Hartschuh A and Novotny L 2003 *Phys. Rev. Lett.* **90** 13903
[17] Bouhelier A, Beversluis M R and Novotny L 2003 *Appl. Phys. Lett.* **82** 4596
[18] Quabis S, Dorn R, Glöckl O, Reichle M and Eberler M 2000 *Opt. Commun.* **179** 1
[19] Karrai K and Grober R D 1995 *Appl. Phys. Lett.* **66** 1842
[20] Kapkiai L K, Nichols D M, Carnell J, Krogmeier J R and Dunn R C 2004 *Appl. Phys. Lett.* **84** 3750
[21] Koopman M, de Bakker B I, Garcia-Parajo M F and van Hulst N F 2004 *Appl. Phys. Lett.* **83** 5083
[22] Anderson N, Hartschuh A, Cronin S and Novotny L 2005 *J. Am. Chem. Soc.* **127** 2533
[23] Saito R, Dresselhaus G and Dresselhaus M S 1998 *Physical Properties of Carbon Nanotubes* (London: Imperial College Press)
[24] Reich S, Thomsen C and Maultzsch J 2004 *Carbon Nanotubes: Basic Concepts and Physical Properties* (Weinheim: Wiley–VCH)
[25] Mews A, Koberling F, Basche T, Philipp G, Duesberg G S, Roth S and Burghead M 2000 *Adv. Mater.* **12** 1210
[26] Maultzsch J, Reich S and Thomsen C 2001 *Phys. Rev.* B **64** 121407
[27] Hartschuh A, Hermeneglido N P, Novotny L and Krauss T D 2003 *Science* **301** 1354
[28] Rao A M *et al* 1997 *Science* **275** 187
[29] Jorio A, Saito R, Hafner J H, Lieber C M, Hunter M, McClure T, Dresselhaus G and Dresselhaus M S 2001 *Phys. Rev. Lett.* **86** 1118
[30] Souza M *et al* 2004 *Phys. Rev.* B **69** 241403
[31] Fantini C, Jorio A, Souza M, Ladeira L O, Souza Filho A G, Samsonidze Ge G, Dresselhaus G, Dresselhaus M S and Pimenta M A 2004 *Phys. Rev. Lett.* **93** 087401
[32] Fantini C, Jorio A, Souza M, Strano M S, Dresselhaus M S and Pimenta M A 2004 *Phys. Rev. Lett.* **93** 147406
[33] Anderson N, Hartschuh A and Novotny L 2005 *Mater. Today* **54** (May)
[34] Kreibig U and Vollmer M 1994 *Optical Properties of Metal Clusters* (Berlin: Springer)
[35] Bohren C F and Huffman D R 1998 *Absorption and Scattering of Light by Small Particles* (New York: Wiley)
[36] Wiederrecht G P 2004 *Eur. Phys. J. Appl. Phys.* **28** 3–18
[37] Li K, Stockmann M I and Bergman D J 2003 *Phys. Rev. Lett.* **91** 227402
[38] Chicanne C, David T, Quidant R, Weeber J C, Lacroute Y, Bourillot E, Dereux A, Colas des Francs G and Girard C 2002 *Phys. Rev. Lett.* **88** 097402
[39] Ditlbacher H, Krenn J R, Schider G, Leitner A and Aussenegg F R 2002 *Appl. Phys. Lett.* **81** 1762
[40] Wiederrecht G P, Wurtz G A and Hranisavljevic J 2004 *Nano Lett.* **4** 2121
[41] Maier S A, Kik P G, Atwater H A, Meltzer S, Harel E, Koel B E and Requicha A A G 2203 *Nat. Mater.* **1** 852
[42] Mikhailovsky A A, Petruska M A, Stockmann M I and Klimov V I 2003 *Opt. Lett.* **28** 1686
[43] Hillenbrand R, Keilmann F, Hanarp P, Sutherland D S and Aizpurua J 2003 *Appl. Phys. Lett.* **83** 368
[44] Bouhelier A, Beversluis M R and Novotny L 2003 *Appl. Phys. Lett.* **83** 5041
[45] Imura K, Nagahara T and Okamoto H 2004 *J. Am. Chem. Soc.* **126** 12730
[46] Imura K, Nagahara T and Okamoto H 2004 *J. Phys. Chem.* B **108** 16344
[47] Boyd G T, Yu Z H and Shen Y R 1986 *Phys. Rev.* B **33** 7923
[48] Beversluis M R, Bouhelier A and Novotny L 2003 *Phys. Rev.* B **68** 115433
[49] Schuck P J, Fromm D P, Sundaramurthy A, Kino G S and Moerner W E 2005 *Phys. Rev. Lett.* **94** 017402
[50] Mühlschegel P, Eisler H J, Martin O J F, Hecht B and Pohl D W 2005 *Science* **308** 1607